inorganics

MDPI

Article

Impregnation of Synthetic Saponites with Aldehydes: A Green Approach in the Intercalation of Bioactive Principles

Stefano Marchesi [1], Geo Paul [1], Matteo Guidotti [2], Stefano Econdi [2,3], Chiara Bisio [1,2,*] and Fabio Carniato [1,*]

[1] Dipartimento di Scienze e Innovazione Tecnologica, Università degli Studi del Piemonte Orientale "Amedeo Avogadro", Viale Teresa Michel 11, 15121 Alessandria, Italy
[2] CNR-SCITEC Istituto di Scienze e Tecnologie Chimiche "G. Natta", Via C. Golgi 19, 20133 Milano, Italy
[3] Dipartimento di Chimica, Università degli Studi di Milano, Via C. Golgi 19, 20133 Milano, Italy
* Correspondence: chiara.bisio@uniupo.it (C.B.); fabio.carniato@uniupo.it (F.C.); Tel.: +39-0131360216 (C.B.); +39-0131360217 (F.C.)

Abstract: Synthetic saponite clay was impregnated with either linear saturated or unsaturated aldehydes through an incipient-wetness deposition approach. To increase the aldehyde loading, saponite was also intercalated with positively charged cetyltrimethylammonium (CTA^+) species, aiming to expand the clay gallery and to increase the hydrophobic character of the host solid. A multitechnique, physicochemical investigation was performed on the organic–inorganic hybrid solids. The analyses revealed that the aldehydes are mainly adsorbed on the clay particles' surface, with a small fraction inside the interlayer space. In CTA^+-modified saponites, the concentration of saturated aldehydes was higher than the one observed in the pure clay. These features are quite promising for the development of novel layered solids containing bioactive molecules for ecocompatible and economically sustainable applications, especially in agriculture, for the development of innovative hybrid materials for crop protection.

Keywords: synthetic clay; saponite; cetyl trimethyl ammonium; aldehyde; organic/inorganic hybrid material; agriculture

Citation: Marchesi, S.; Paul, G.; Guidotti, M.; Econdi, S.; Bisio, C.; Carniato, F. Impregnation of Synthetic Saponites with Aldehydes: A Green Approach in the Intercalation of Bioactive Principles. *Inorganics* **2022**, *10*, 159. https://doi.org/10.3390/inorganics10100159

Academic Editor: Carlos Martínez-Boubeta

Received: 29 August 2022
Accepted: 26 September 2022
Published: 29 September 2022

1. Introduction

Synthetic saponite clays represent a class of smectite-type hydrated phyllosilicate materials, consisting of a 2:1 trioctahedral structure of alternating tetrahedral (T) and octahedral (O) sheets typically composed of Si(IV), Al(III), Mg(II) and O^{2-} sites, organized to form T-O-T layers alternating with an interlamellar space containing exchangeable cations and water molecules (Scheme S1) [1–4]. Compared to their natural mineral counterparts, these systems present several advantages, such as a more controlled chemical composition, well-defined physicochemical properties, high mechanical robustness and thermal stability, relatively low production costs and high chemical versatility [4–9]. For these reasons, synthetic saponites have attracted growing interest by the scientific community and novel derivative samples have been prepared and proposed for different scientific and technological applications, spanning from biomedicine [4,10,11] to catalysis [3,4,12–14], together with environmental [4,15–18] and energy-related purposes [3,4,19,20]. The physicochemical features of saponites can be modulated at three different levels: (1) modification of the composition, structure and morphology by varying the dilution of the synthesis gel in the hydrothermal synthesis [3–5,16,21] or by following alternative synthetic procedures based on sol-gel and microwave-assisted reactions [4,9,22–24]; (2) introduction into the lamellae framework of metal ions, in order to confer specific properties to the final materials [4,25–32]; (3) modification of the interlayer space of saponite, through intercalation of different chemical entities (i.e., ions, organic substances, metallo-chelates) [3,4,33–37].

For these reasons, saponites represent an interesting 2D aluminosilicate platform with very high chemical versatility and huge potential application in many scientific and technological fields. For example, the confinement of simple and light active organic molecules in a clay matrix could be a good strategy to obtain new materials of interest for agronomic applications. Medium-chain linear aldehydes, in fact, such as *n*-hexanal, *n*-heptanal, *[E]*-hex-2-enal and *[E]*-hept-2-enal, are bioactive molecules with a marked repellent and/or signaling activity on pests and parasitic organisms for crops. These C_7- and C_6-aldehydes, in particular, are effective semiochemicals and repellants against the olive fly, *Bactrocera oleae*, and are finding a growing application in protection of olive-tree crops [38–41].

Saponite clay could represent a good tool for the deposition, immobilization and gradual release of bioactive chemicals in open-field application, reducing the local concentration of active species, eliminating the use of organic solvents as carriers, mitigating washout and weathering by rain and hot climates and limiting environmental impact. Moreover, saponite itself is an ecocompatible solid, considering that it is a synthetic analog of clay minerals.

Based on these considerations, a synthetic saponite clay (Sap) was employed in this study as the inorganic support for the immobilization of four aldehydes, either saturated or unsaturated (*n*-hexanal, *n*-heptanal, *[E]*-hex-2-enal and *[E]*-hept-2-enal) through an incipient-wetness deposition approach. To increase the final load of active aldehydes, a set of organically modified saponites (CTASap) was also prepared, and the final properties of these organic–inorganic hybrid systems were investigated though a physicochemical multitechnique approach.

2. Results and Discussion

2.1. Impregnation of Synthetic Saponite with Saturated and Unsaturated Aldehydes

A synthetic saponite clay (Sap) was synthesized through a classical hydrothermal method [4,16,17], with a H_2O/Si molar ratio of 20 (Scheme S1). The gel dilution led to a final layered solid with micrometer-sized particles [16,21] and a high cation-exchange capacity (CEC), 75.2 $\pm$ 5.5 meq/100 g, as determined by the standard UV–Vis method with hexamminecobalt(III) chloride [42] (Figure S1). The material is composed of lamellae with different spatial organization (Figure S2A) and a specific surface area (SSA) of 210 $m^2\ g^{-1}$, as estimated by applying the Brunauer–Emmett–Teller (BET) algorithm to the N_2 physisorption isotherm (Figure S2B). The sample is characterized by a type IV isotherm, common to materials composed of micro- and mesopores, with H3 hysteresis loops, due to presence of heterogeneous mesopores generated by the lamellae aggregation [16].

The saponite was then impregnated with aliphatic saturated (*n*-hexanal, C6AN, *n*-heptanal, C7AN) or unsaturated (*[E]*-hex-2-enal, C6EN, *[E]*-hept-2-enal, C7EN) aldehydes via an incipient-wetness deposition method (Scheme S2), as described in detail in Section 3.1.2. The physicochemical properties of the hybrid solids (hereafter named SapC6AN, SapC7AN, SapC6EN and SapC7EN, respectively) were carefully investigated by using different techniques.

The content of aldehydes immobilized in the solid was determined by CHN elemental analysis. CHN measurements were performed on SapC6AN, SapC7AN, SapC6EN and SApC7EN every 10 days up to 30 days, in order to evaluate the persistence of the impregnated organic compounds in the synthetic clay and its gradual release into the atmosphere (Figure 1). A high concentration of C7AN was found in the SapC7AN sample (Figure 1d) with a starting value of ca. 18 wt. %, followed by the samples loaded with C6EN (Figure 1c) and C7EN (Figure 1b) with values of 12.18 and 11.75 wt. %, respectively. In contrast, SapC6AN contains a small amount of aldehyde (Figure 1a), close to 6.38 wt. %. The variable amount of the four aldehydes may be attributed to their different volatility and chemical affinity with the inorganic support [43–46]. After 30 days, SapC6AN showed a 0.62 wt. % decrease in the aldehyde content, comparable to the one observed for SapC6EN. For SapC7AN and SapC7EN solids, a diminution of 2.12 and 2.00 wt. %, respectively, was

observed. Considering that the binding capacity is based on weak, noncovalent interactions (Scheme 1) and that the main route of aldehyde release is evaporation, the main factor influencing the release of the bioactive species from the solid is temperature, which promotes volatilization and removal of the aldehyde.

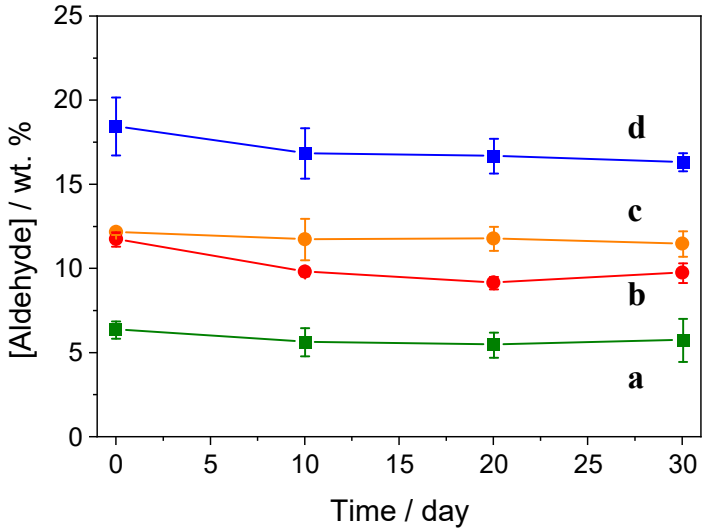

Figure 1. Content of aldehydes (as wt. %) during a period of 30 days in the saponite samples: a = SapC6AN, b = SapC7EN, c = SapC6EN, d = SapC7AN. The aldehyde content was measured by CHN elemental analyses. Environmental conditions: open air, 25 °C, atmospheric pressure.

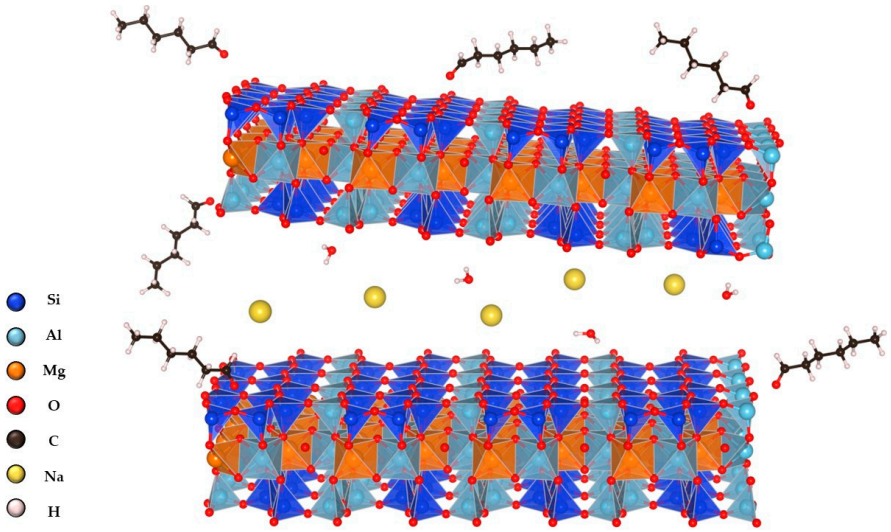

Scheme 1. Schematic view of the distribution of C6AN aldehyde on the saponite surface.

The structural properties of the saponite before and after the impregnation process with the aldehydes were investigated by X-ray powder diffraction (XRPD) (Figure 2). The X-ray pattern of the as-synthesized Sap shows the typical reflections of a smectite clay (Figure S3), defined by the reflections attributed to the (001), (110)–(020), (004), (130)–(201), (311) and (060) crystalline planes [4,16,17]. In particular, the position of the (060) plane at 60.5° 2θ is indicative of the 2:1 T-O-T trioctahedral layered structure of the clay [1], while the (001) basal plane of the saponite, with a reflection at ca. 6° 2θ, is indicative of the thickness of the T-O-T structure plus the interlayer space [3,4]. After impregnation with the aldehydes, the basal reflection becomes more defined and this is mainly evident for the SapC7AN sample (Figure 2b–e), thus indicating an increase in the order of structural packing [5]. The small increase in the interlayer space in the aldehyde-containing clays suggests that a limited fraction of aldehydes is confined in the saponite gallery. Additionally,

an important component of the organic molecules may be adsorbed on the external surface of the clay particles, interacting through dispersion and dipole–dipole forces with saponite (Scheme 1).

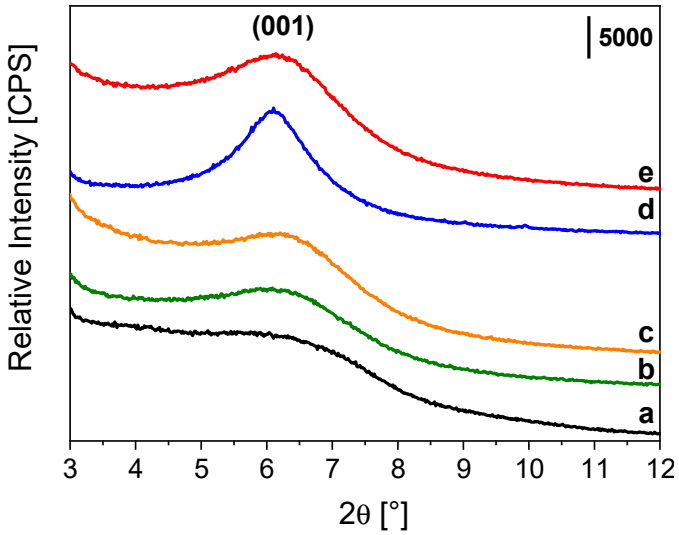

Figure 2. Diffractograms of saponite samples before and after impregnation with the aldehydes, collected in the 3–12° 2θ range: Sap (a), SapC6AN (b), SapC6EN (c), SapC7AN (d) and SapC7EN (e).

The thermal behavior of the impregnated saponites was studied through variable-temperature infrared spectroscopy (VT FTIR) experiments. The IR spectra of SapC6AN, SapC6EN, SapC7AN and SapC7EN samples were measured in vacuum from 30 to 500 °C on self-supporting pellets (Figures 3B and S4B–S6B). The spectra collected at 30 °C were compared with the one of Sap (Figures 3A and S3A–S5A) to better identify the signals attributed to the aldehydes. The IR spectrum of SapC6AN (Figure 3Ab) shows, along with the typical signals of the smectite support, the asymmetric and symmetric stretching (located at 2960–2870 cm^{-1}) and bending (at ca. 1470–1340 cm^{-1}) modes of $–CH_3$ and $–CH_2$ groups of the aldehyde. Moreover, the peaks associated with the C-H stretching of the carbonyl group and the C=O stretching are present at 2750 and 1715 cm^{-1}, respectively [1,5,35,47,48].

A comparable set of IR bands were observed in the spectra of SapC6EN (Figure S4Ab), SapC7AN (Figure S5Ab) and SapC7EN (Figure S6Ab). The spectra of SapC6EN and SapC7EN also present the signals in the 1680–1660 cm^{-1} range related to the C=C stretching modes. The variable-temperature IR measurements of the four samples (Figures 3B and S4B–S6B) show the beginning of the degradation of aldehydes ca. 250–300 °C (ca. 100–150 °C above the boiling point of the pure aldehydes [43–46]), as indicated by the initial erosion of the stretching modes of the organic groups described above, and the occurrence of a new band at ca. 1600 cm^{-1}, assigned to the carbonization of the organic fraction. The thermal treatment led to the elimination of physisorbed water from the solids, with a marked diminution of the related bands (3500–3100 and 1640 cm^{-1}). A further decrease in aldehydes bands is observed with increasing temperature. However, even at 500 °C, there is still the presence of low-intensity signals associated with the organic compounds in carbonization structures. These results clearly indicate a crucial role of the saponite structure in the thermal stabilization of the saturated and unsaturated aldehydes, when adsorbed on the smectite's surface [49,50].

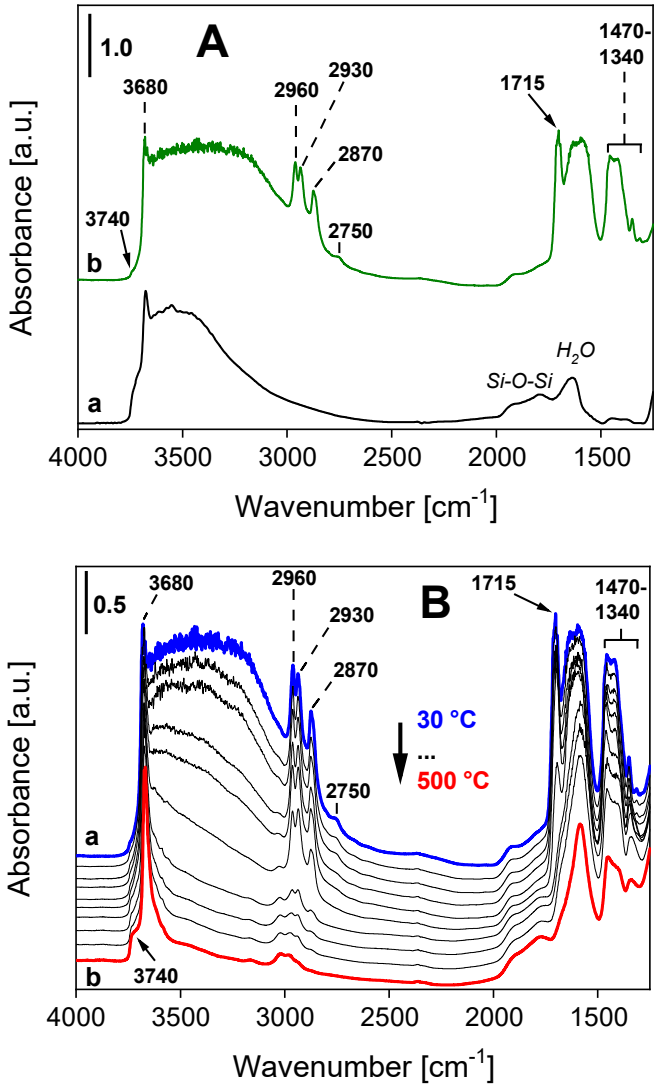

Figure 3. (**A**) FTIR spectra, in the 4000-1250 cm^{-1} region, of the Sap (a) and SapC6AN (b) samples, measured in vacuo at room temperature on self-supporting pellets. (**B**) Variable temperature FTIR spectra of the SapC6AN sample, measured in vacuo on a self-supporting pellet, from 30 °C (a) to 500 °C (b).

Lastly, ^{1}H ECHO MAS and ^{13}C CPMAS NMR (Figure 4) analyses were performed to confirm the successful incorporation of aldehydes within the saponite clays. There are two sets of overlapped proton peaks visible in the ^{1}H ECHO NMR spectra (Figure 4A) that are associated with saponite backbone and to adsorbed aldehydes. The peak at 0.5 ppm is due to Al-OH and Mg-OH groups, while the peak belongs to silanols appears at 1.9 ppm (Figure 4A) [51]. In addition, an intense and relatively broad peak observed at 4.9 ppm is assigned to physisorbed water. Moreover, all spectra exhibited peaks associated with aldehydes (v. assignations in Figure 4A). Peaks associated with protons bound to unsaturated carbons (around 6 and 7 ppm) are also found in the spectra of SapC6EN and SapC7EN (Figure 4A(c, d)). Although the presence of aldehyde molecules can be confirmed from ^{1}H NMR data, substantially low loading of these molecules is evident in the spectra. In contrast, further structural information can be derived from the ^{13}C CPMAS NMR spectra (Figure 4B). Distinct ^{13}C peaks are observed in the spectra, proving the successful incorporation of the aldehyde in saponite clays using the incipient-wetness deposition approach, and the displayed peaks are assigned to the structure of the aldehydes. Sharp resonances associated with the impregnated species indicate that the molecules are mobile and experience weaker interactions with the host saponite surfaces [52,53].

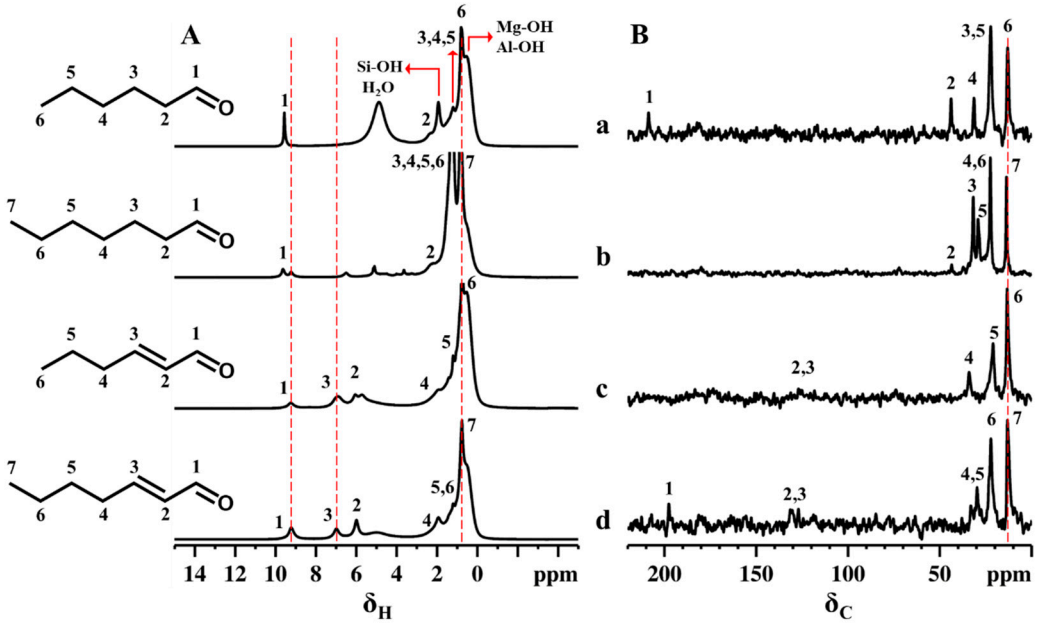

Figure 4. ^{1}H ECHO (**A**) and ^{13}C CPMAS (**B**) NMR spectra of SapC6AN (a), SapC7AN (b), SapC6EN (c) and SapC7EN (d) samples.

2.2. CTA-Intercalated Synthetic Saponite Clays Impregnated with Saturated Aldehydes

To improve the amount of aldehyde molecules immobilized in the solid support, a Na^+-exchanged saponite derivative (NaSap, Scheme S1) was submitted to a subsequent cation-exchange process with the cationic quaternary ammonium surfactant cetyltrimethylammonium bromide, producing the sample named CTASap. This procedure ensures the intercalation of CTA^+ species inside the interlayer space of the clay, replacing Na^+ ions [35]. Moreover, the presence of CTA^+ species in the saponite allows for increasing both (i) the interlamellar distance and (ii) the hydrophobicity of the clay in such a way as to increase its affinity with the uncharged nonpolar aldehydes and, thus, potentially increasing the concentration of organic molecules incorporated in the inorganic host during the impregnation [54–60].

The CTASap was then impregnated with two saturated aldehydes, producing two final samples named CTASapC6AN and CTASapC7AN. The amount of cationic CTA^+ groups in the CTASap sample was estimated from CHN elemental analysis to be 0.61 mmol/g (Table S1). The amount of CTA^+ confined in the saponite was also estimated by thermogravimetric (TG) analysis: an amount of 0.68 mmol/g of surfactant, hence in good agreement with CHN data (Table S2), was extrapolated from the overall weight loss assigned to the surfactant decomposition between 200 and 700 °C (Figure S7A,B). In the TG curves, a shoulder at 260 °C suggests the presence of a small fraction of nonintercalated CTA^+ molecules (1.73 wt. %). Additionally, the weight loss with maximum at 360 °C is associated with the degradation of the intercalated CTA^+ chains, which is 60 °C greater than the decomposition temperature of the pure CTA^+ molecule [35], while the weight loss in the 430–700 °C range was attributed to the complete degradation of the intercalated surfactant groups and charring byproducts. As previously found [35,49,50], the saponite structure has an active role in the thermal stabilization and protection of CTA, influencing its thermal degradation pathway. The comparison of TG profiles of NaSap and CTASap clearly shows that the latter contained a lower amount of physisorbed water than the former (1.8 wt. % vs. 5.1 wt. %), owing to its greater hydrophobic character [35].

TG data were supported by VT FTIR measurements carried out on the CTASap sample from 30 to 500 °C (Figure S8). The IR spectrum of the organically modified sample shows a gradual erosion of the bands typical of the CTA^+ units (C-H asymmetric and symmetric stretching modes, between ca. 3100 and 2800 cm^{-1}, and bending vibrations, between ca. 1500 and 1300 cm^{-1}) in the 250–500 °C range [35,48].

The concentration of saturated aldehydes in the CTASapC6AN and CTASapC7AN solids increased compared to the parent SapC6AN and SapC7AN, equal to +105% and +22%, respectively (Figure 5). This effect can be due to the greater hydrophobic character of CTASap compared to unmodified Sap, which facilitates adsorption of the two aldehydes on the particle surface.

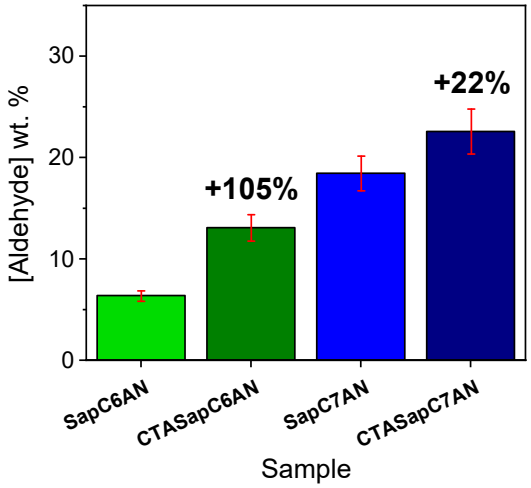

Figure 5. Increment of C6AN and C7AN aldehyde content in the related CTASap samples, compared to the parent solids. Aldehyde content was measured by CHN analysis.

The effect of the introduction of CTA^+ ions and the additional insertion of C6AN and C7AN aldehydes in the saponite matrix was investigated by X-ray diffraction. A marked increase in the basal $d_{(001)}$-spacing was observed with the intercalation of CTA^+ groups with a shift of the (001) reflection from ca. 7.7° 2θ ($d_{(001)}$-spacing = 1.15 nm) of NaSap to ca. 6.1° 2θ ($d_{(001)}$-spacing = 1.46 nm) of CTASap (Figure 6) [34,35,61]. After addition of C6AN or C7AN aldehydes the (001) plane further increases, with a new $d_{(001)}$-spacing value of 1.52 and 1.48 nm, respectively. However, as also observed for the parent SapC6AN and SapC7AN, the increment of the *d*-spacing value is limited, testifying that a large fraction of aldehydes is yet confined on the external surface of saponite.

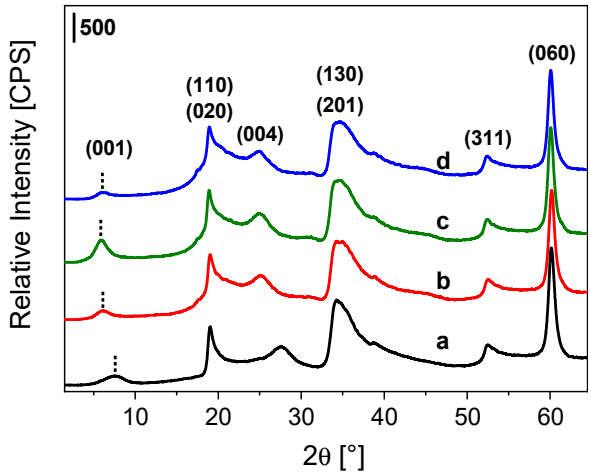

Figure 6. Diffractograms collected in the 1.5–65° 2θ range of NaSap (a), CTASap (b), CTASapC6AN (c) and CTASapC7AN (d) samples.

Finally, in Figure 7 we show the NMR spectra of CTA-intercalated synthetic saponite clays with added saturated aldehydes. The ^{1}H ECHO NMR spectra are dominated by the protonic contributions from CTA cations and inorganic protons (Mg-OH, Al-OH and Si-OH) [35]. However, the presence of impregnated species can be confirmed through

the detection of aldehydic protons at ca. 9.2 and 9.6 ppm. Furthermore, the presence of multiple ^{1}H peaks for unique aldehydic protons in CTASapC6AN and CTASapC7AN can be attributed to different binding environments for impregnated molecules. Furthermore, due to the higher aldehyde loading in CTASapC7AN, the peaks associated with inorganic protons displayed low intensity (Figure 7A(b)). Figure 7B shows the ^{13}C CPMAS NMR spectra of CTASapC6AN and CTASapC7AN, which is effectively populated with peaks of CTA molecules [35]. However, peaks associated with the impregnated aldehyde species can be clearly detected through their characteristic ^{13}C peaks (Figure S9). The coexistence of both *trans* (around 32.5 ppm) and *gauche* (around 30.5 ppm) conformations of CTA^{+} molecules are noted through the chemical shift of methylene carbons; however, the extraction of further details are complicated due to the overlapping of peaks from aldehydes and CTA^{+}. The better signal/noise ratio observed in the ^{1}H and ^{13}C NMR spectra confirms significant loading of aldehydes in CTA-intercalated saponite clays by using the incipient-wetness deposition approach.

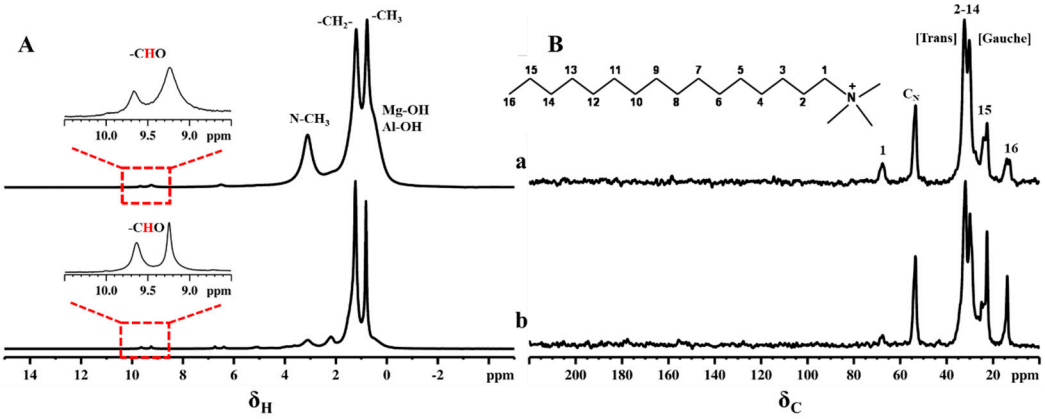

Figure 7. ^{1}H ECHO (**A**) and ^{13}C CPMAS (**B**) NMR spectra of CTASapC6AN (a) and CTASapC7AN (b) samples.

3. Materials and Methods

3.1. Materials

3.1.1. Synthesis of Sap and NaSap Clays

Synthetic saponite clay with high cationic exchange capacity (CEC = 75.2 ± 5.5 meq/100 g) was synthesized following a classical hydrothermal method, previously optimized in our laboratories [4,16,17], with SiO_2:MgO:Al_2O_3:Na_2O:H_2O molar composition for the synthesis gel: 1:0.835:0.056:0.056:20 (H_2O/Si ratio of 20) (Scheme S1).

In detail, 5.95 g of silica fumed (SiO_2; 0.095 mol; 99.8%, Sigma-Aldrich, Burlington, MA, USA) was added in 29.1 mL of aqueous 0.4 M sodium hydroxide solution (NaOH; 0.010 mol; Sigma-Aldrich, Burlington, MA, USA), and the resulting gel was stirred at room temperature for 1 h. Afterward, 18.8 g of magnesium acetate tetrahydrate ($Mg(CH_3COO)_2 \cdot 4H_2O$; 0.090 mol; 99%, Sigma-Aldrich, Burlington, MA, USA), 2.3 g of aluminum *iso*-propoxide ($Al[OCH(CH_3)_2]_3$; 0.010 mol; 98%, Sigma-Aldrich, Burlington, MA, USA) and 8.2 mL of ultrapure water were added to the gel. After 2 h of stirring, the mixture was transferred into a PTFE cup (125 mL capacity) inside an autoclave (Anton Paar 4748) and treated at 513 K for 72 h. The final solid, Sap, was then filtered and washed with ultrapure water until neutral pH was reached, and finally dried at 100 °C overnight.

The Na^{+}-exchanged synthetic saponite clay was prepared as follows (Scheme S1): 2 g of Sap clay was dispersed in 200 mL of saturated sodium chloride (NaCl; Sigma-Aldrich, Burlington, MA, USA) solution for 36 h at room temperature. This procedure allows replacement of the cations present in the interlayer space (i.e., Al^{3+}, Mg^{2+}, H^{+}) with Na^{+}. The final solid, NaSap, was then washed with hot ultrapure water via centrifugation until complete elimination of chlorides (confirmed by silver nitrate spot test), and finally dried at 100 °C overnight.

3.1.2. Impregnation of Saturated and Unsaturated Aldehydes on Saponite Clay

Aldehyde-containing saponite solids were prepared by means of an incipient-wetness approach. Linear saturated and unsaturated aldehydes were used, namely: *n*-hexanal (C6AN, ≥97%, Sigma-Aldrich, Burlington, MA, USA), *n*-heptanal (C7AN, ≥95%, Sigma-Aldrich, Burlington, MA, USA), *[E]*-hex-2-enal (C6EN, ≥97%, TCI, Tokyo, Japan), *[E]*-hept-2-enal (C7EN, ≥95%, TCI, Tokyo, Japan) (Scheme S2).

The support material Sap clay (2.40 g) was pretreated before contact with the aldehydes by drying it at 110 °C for 3 h and then left to cool for 30 min under N_2 purging. The impregnation solution was prepared by mixing 1.50 mL of petroleum ether 40/60 (Sigma-Aldrich, Burlington, MA, USA) with 105 mmol of the desired aldehyde (0.130 mL C6AN, 0.150 mL C7AN, 0.128 mL C6EN or 0.145 mL C7EN). The prepared solution was gently and uniformly poured on the clay and the impregnated solid was thoroughly mixed. The solid was left to dry by stirring under a fume hood for ca. 6 h at room temperature to allow a complete spontaneous evaporation of the petroleum ether 40/60 solvent. The final solid was stored under anhydrous conditions. Four materials were accordingly obtained: SapC6AN (Sap + *n*-hexanal), SapC7AN (Sap + *n*-heptanal), SapC6EN (Sap + *[E]*-hex-2-enal) and SapC7EN (Sap + *[E]*-hept-2-enal).

3.1.3. Intercalation of CTA^+ Groups in Na-Saponite Clay

The intercalation process of cationic hexadecyltrimethylammonium bromide (CTAB; ≥98%, Sigma-Aldrich, Burlington, MA, USA) species inside the interlayer space of NaSap clay was performed following the procedure published in the literature by Bisio et al. [35].

In detail, 2.5 g of NaSap clay was dispersed in a solution composed of 0.5 g of CTAB (1.4 mmol) in 50 mL of ultrapure water, and then stirred at room temperature for 36 h. After treatment, the solid suspension was filtered and finally dried at 100 °C overnight, obtaining the solid named CTASap.

3.1.4. Impregnation of Saturated Aldehydes on CTASap Clay

The preparation of CTASap samples impregnated with C6AN and C7AN aldehydes (hereafter indicated as CTASapC6AN and CTASapC7AN, respectively) followed the same protocol described in the Section 3.1.2.

3.2. Analytical Methods

The cationic exchange capacity (CEC) parameter of saponite clay was determined by the ultraviolet–visible (UV–Vis) method as reported in the literature [42]. In detail, 0.300 g of NaSap sample was exchanged with 10 mL of a 0.02 M hexamminecobalt(III) chloride ($[Co(NH_3)_6]^{3+}$) solution at 298 K for 60 h. After separation by centrifugation, the solution was analyzed by UV–Vis spectroscopy. UV–Vis spectra were recorded at 298 K in the range 300–600 nm with a resolution of 1 nm, using a double-beam Perkin Elmer Lambda 900 Spectrophotometer (Perkin Elmer, Waltham, MA, USA). The absorbance of the band at 475 nm ($^1A_{1g} \rightarrow {}^1T_{1g}$) [62], relative to a *d-d* spin-allowed Laporte-forbidden transition of Co^{3+}, was evaluated to quantify the amount of Co^{3+} ions free in solution, thereby determining the amount exchanged in the procedure and thus the CEC of the clay. $[Co(NH_3)_6]^{3+}$ standard aqueous solutions, in the concentration range 0.05–0.005 M, were measured at room temperature.

CHN elemental analyses were accomplished with an EA3000 CHN Elemental Analyzer (EuroVector, Milano, Italy). Acetanilide, purchased from EuroVector (Milano, Italy), was used as the calibration standard (C % = 71.089, H % = 6.711, N % = 10.363).

X-ray powder diffractograms (XRPD) were collected on unoriented ground powders using a Bruker D8 Advance Powder Diffractometer (Karlsruhe, Germany), operating in Bragg–Brentano geometry, with Cu anode target equipped with a Ni filter (used as X-ray source) and with a Lynxeye XE-T high-resolution position-sensitive detector. Trio and Twin/Twin optics are mounted on the DaVinci Design modular XRD system. The X-ray tube of the instrument operates with a Cu-$K_{\alpha 1}$ monochromatic radiation (λ = 1.54062 Å),

with the current intensity and operative electric potential difference set to 40 mA and 40 kV, respectively, and with automatic variable primary divergent slits and primary and secondary Soller slits of 2.5°. The X-ray profiles were recorded at room temperature in the 2°–65° 2θ range with a coupled 2θ–θ method, continuous PSD fast scan mode, time per step (rate or scan speed) of 0.100 s/step, 2θ step size (or increment) of 0.01°, with automatic synchronization of the air scatter (or antiscatter) knife and slits and with fixed illumination sample set at 15 mm.

Thermogravimetric analyses (TGA) were carried out with a Setaram SETSYS Evolution Thermobalance (Caluire, France). The TG curves were collected in the temperature range 25–1100 °C at 3 °C/min scan rate, using argon as the analysis (or carrier) gas with a flow of 20 mL/min and argon as the purge (or protective) gas.

Fourier-transform infrared (FTIR) spectra were collected on a Bruker Equinox 55 Spectrometer (Billerica, MA, USA) in the range 4000–400 cm^{-1} with a resolution of 4 cm^{-1}. Self-supporting pellets of solid samples were placed into a specialized IR cell equipped with potassium bromide (KBr) windows, permanently connected to a vacuum line (residual pressure lower than 10^{-4} mbar). All samples were first measured in vacuo at room temperature. For the aldehyde-containing samples, the experimental setup adopted allowed all temperature treatment experiments to be carried out in situ. FTIR spectra were collected by heating the samples from 30 to 500 °C. The spectra were normalized by taking as a reference the intensity of the overtones and combination modes of the siloxane framework (bands in the 2000–1700 cm^{-1} range). In this manner, differences in the intensity of the bands across different samples related to intrinsic oscillators of the materials (i.e., hydroxyl groups, -OH) can be associated with actual differences in the amount of these species in the samples. Because of the normalization, the absorbance values are reported in arbitrary units, a.u.

Solid-state NMR (ssNMR) spectra were acquired with a wide-bore, 11.74 T magnet and a Bruker Avance III 500 Spectrometer (Rheinstetten, Germany) equipped with a 4 mm triple resonance probe in double resonance mode. Powdered samples were packed on a zirconia rotor and closed with Kel-F cap and spun at a magic angle spinning (MAS) rate of 10–15 kHz, at 300 K. A rotor-synchronized ^{1}H spin–echo sequence (π/2–τ–π–τ–acquisition) was applied to record the ^{1}H NMR spectra with delay time τ of 666 ms. The magnitude of radio frequency (RF) pulse was set at 100 kHz. For the ^{13}C CPMAS experiments, the initial excitation and decoupling proton radio frequencies (RF) were 55 and 28 kHz, respectively. During the CP period the ^{1}H RF field was ramped using 100 increments, whereas the ^{13}C RF field was maintained at a constant level. A moderately ramped RF field of 55 kHz was used for spin locking, while the carbon RF field was matched to obtain an optimal signal (40 kHz) and a CP contact time of 5 ms was employed. During the acquisition, the protons were decoupled from the carbons by using a TPPM-15 decoupling scheme. The relaxation delay, d1, between accumulations was 3s for ^{1}H MAS and for ^{13}C CPMAS experiments. All chemical shifts are reported by externally referencing to TMS at 0 ppm.

4. Conclusions

In this work, a series of synthetic saponite clays impregnated with linear saturated (*n*-hexanal and *n*-heptanal) and unsaturated (*[E]*-hex-2-enal and *[E]*-hept-2-enal) aldehydes were successfully prepared through the incipient-wetness method. Structural analyses on the aldehydes-loaded saponites showed that the organic substances are mainly adsorbed on the clay surface, with a small fraction possibly intercalated in the interlayer space. In addition, the organic molecules are highly mobile and experience weaker interactions with the inorganic host surfaces. The aldehyde content is different in the solids, depending on their chemical properties and affinity with the host material. Furthermore, the guest molecules are thermally stabilized by the saponite. Subsequently, the intercalation of CTA^{+} species in the saponite led to a significant increase in the size of the interlayer space, improving at the same time the hydrophobicity and thus the adsorption capacity of the clay. The concentration of the guest saturated aldehydes increases in the organically modified

saponite with respect to the one in unmodified parent solids. It appears that a fraction of the aldehyde is retained in the vicinity or be partially inside the interlayer space of the host clay, owing to favorable interactions with the CTA^+ groups, while a significant portion of it is still physisorbed onto the particle surface of the hybrid material. The information collected in this study represents an interesting starting point for the design of novel layered solids containing bioactive molecules for low environmental impact and economically sustainable applications in many sectors of the applied sciences, such as the protection of agricultural crops and the targeted delivery of phytopharmaceutically active molecules. Clearly, only preliminary open-field trials can confirm the efficacy of the treatment and, in case of unsatisfactory data, higher doses of material or more frequent treatments can be planned.

Supplementary Materials: The following supporting information can be downloaded at: https://www.mdpi.com/article/10.3390/inorganics10100159/s1, Scheme S1: Schematic representation of the hydrothermal synthesis of synthetic saponite clays SAP-20 (Sap) and Na-SAP-20 (NaSap), prepared with a H_2O/Si ratio of 20; Figure S1: (A) UV–Vis spectra of $[Co(NH_3)_6]^{3+}$ standard aqueous solutions at room temperature (concentration range 0.05–0.005 M) used for the calibration curve. (B) Calibration curve derived from UV–Vis spectra of the standard solutions (λ_{abs} = 475 nm). (C) UV–Vis spectrum of the NaSap sample supernatant, obtained after treatment of the solid in 0.02 M $[Co(NH_3)_6]^{3+}$ aqueous solution at room temperature for 60 h; the curve represents the average spectrum obtained after 3 replicates; Figure S2: (A) TEM micrograph of NaSap sample. (B) N_2 adsorption/desorption isotherm at 77 K of NaSap; Scheme S2: Schematic view of the immobilization procedure of different saturated (*n*-hexanal or C6AN, *n*-heptanal or C7AN) and unsaturated (*[E]*-hex-2-enal or C6EN, *[E]*-hept-2-enal or C7EN) aldehydes in the pristine Sap clay; Figure S3: X-ray powder diffraction profile of Sap sample, recorded in the 2–65° 2θ range. Magnification of the 2–15° 2θ region, in which the (001) basal plane is present, is reported in the inset; Figure S4: (A) FTIR spectra, in the 4000–1250 cm^{-1} region, of Sap (a) and SapC6EN (b) samples, measured in vacuum at room temperature on self-supporting pellets. (B) Variable temperature FTIR spectra of SapC6EN sample, measured in vacuum on a self-supporting pellet, from 30 °C (a) to 500 °C (b); Figure S5: (A) FTIR spectra, in the 4000–1250 cm^{-1} region, of Sap (a) and SapC7AN (b) samples, measured in vacuum at room temperature on self-supporting pellets. (B) Variable temperature FTIR spectra of SapC7AN sample, measured in vacuum on a self-supporting pellet, from 30 °C (a) to 500 °C (b); Figure S6: (A) FTIR spectra, in the 4000–1250 cm^{-1} region, of Sap (a) and SapC7EN (b) samples, measured in vacuum at room temperature on self-supporting pellets. (B) Variable temperature FTIR spectra of SapC7EN sample, measured in vacuo on a self-supporting pellet, from 30 °C (a) to 500 °C (b); Figure S7: TG (A) and DTG (B) curves of NaSap (a) and CTASap (b) samples. The thermogravimetric analyses were carried out under argon flow; Figure S8: Variable temperature FTIR spectra of CTASap sample, measured in vacuo on a self-supporting pellet, from 30 °C (a) to 500 °C (b); Figure S9: ^{13}C CPMAS NMR spectra of CTASap (a), SapC7AN (b) and CTASapC7AN (c) samples. Only the aliphatic region is shown. Inset shows the molecular structure of CTA^+ and C7AN molecules; Table S1: CHN analysis of CTASap; Table S2: CTA^+ content in the CTASap sample obtained from TG analyses shown in Figure S7.

Author Contributions: Conceptualization, S.M., M.G., C.B. and F.C.; methodology, S.M., M.G., S.E., C.B. and F.C.; formal analysis, S.M. and G.P.; investigation, S.M.; data curation, S.M. and G.P.; writing—original draft preparation, S.M.; writing—review and editing, S.M., C.B., M.G., S.E. and F.C. All authors have read and agreed to the published version of the manuscript.

Funding: This research received no external funding.

Data Availability Statement: Not applicable.

Acknowledgments: The authors are fully grateful to Elena Perin (DiSIT, Università del Piemonte Orientale, Alessandria, Italy) for CHN analyses. M.G. and S.E. gratefully acknowledge the Italian Ministry of Agricultural, Food and Forestry Policies, MIPAAF, through the Project 2017-2021 "DIOL—DIfesa da organismi nocivi in OLivicoltura tradizionale e intensiva".

Conflicts of Interest: The authors declare no conflict of interest.

References

1. Kloprogge, J.T.; Ponce, C.P. Spectroscopic Studies of Synthetic and Natural Saponites: A Review. *Minerals* **2021**, *11*, 112. [CrossRef]
2. Kloprogge, J.T.; Komarneni, S.; Amonette, J.E. Synthesis of Smectite Clay Minerals: A Critical Review. *Clays Clay Miner.* **1999**, *47*, 529–554. [CrossRef]
3. Zhou, C.H.; Zhou, Q.; Wu, Q.Q.; Petit, S.; Jiang, X.C.; Xia, S.T.; Li, C.S.; Yu, W.H. Modification, Hybridization and Applications of Saponite: An Overview. *Appl. Clay Sci.* **2019**, *168*, 136–154. [CrossRef]
4. Carniato, F.; Gatti, G.; Bisio, C. An Overview of the Recent Synthesis and Functionalization Methods of Saponite Clay. *New J. Chem.* **2020**, *44*, 9969–9980. [CrossRef]
5. Bisio, C.; Gatti, G.; Boccaleri, E.; Marchese, L.; Superti, G.B.; Pastore, H.O.; Thommes, M. Understanding Physico–Chemical Properties of Saponite Synthetic Clays. *Microporous Mesoporous Mater.* **2008**, *107*, 90–101. [CrossRef]
6. Bisio, C.; Gatti, G.; Boccaleri, E.; Marchese, L.; Bertinetti, L.; Coluccia, S. On the Acidity of Saponite Materials: A Combined HRTEM, FTIR, and Solid-State NMR Study. *Langmuir* **2008**, *24*, 2808–2819. [CrossRef]
7. Blukis, R.; Schindler, M.; Couasnon, T.; Benning, L.G. Mechanism and Control of Saponite Synthesis from a Self-Assembling Nanocrystalline Precursor. *Langmuir* **2022**, *38*, 7678–7688. [CrossRef]
8. Meyer, S.; Bennici, S.; Vaulot, C.; Rigolet, S.; Dzene, L. Influence of the Precursor and the Temperature of Synthesis on the Structure of Saponite. *Clays Clay Miner.* **2020**, *68*, 544–552. [CrossRef]
9. Vogels, R.J.M.J.; Kloprogge, J.T.; Geus, J.W. Synthesis and Characterization of Saponite Clays. *Am. Mineral.* **2005**, *90*, 931–944. [CrossRef]
10. Corbin, G.; Vulliet, E.; Lanson, B.; Rimola, A.; Mignon, P. Adsorption of Pharmaceuticals onto Smectite Clay Minerals: A Combined Experimental and Theoretical Study. *Minerals* **2021**, *11*, 62. [CrossRef]
11. Nisticò, R. A Comprehensive Study on the Applications of Clays into Advanced Technologies, with a Particular Attention on Biomedicine and Environmental Remediation. *Inorganics* **2022**, *10*, 40. [CrossRef]
12. Zhou, C.H. An Overview on Strategies towards Clay-Based Designer Catalysts for Green and Sustainable Catalysis. *Appl. Clay Sci.* **2011**, *53*, 87–96. [CrossRef]
13. Nagendrappa, G. Organic Synthesis Using Clay and Clay-Supported Catalysts. *Appl. Clay Sci.* **2011**, *53*, 106–138. [CrossRef]
14. Tiozzo, C.; Bisio, C.; Carniato, F.; Marchese, L.; Gallo, A.; Ravasio, N.; Psaro, R.; Guidotti, M. Epoxidation with Hydrogen Peroxide of Unsaturated Fatty Acid Methyl Esters over Nb(V)-Silica Catalysts. *Eur. J. Lipid Sci. Technol.* **2013**, *115*, 86–93. [CrossRef]
15. Zhang, T.; Wang, W.; Zhao, Y.; Bai, H.; Wen, T.; Kang, S.; Song, G.; Song, S.; Komarneni, S. Removal of Heavy Metals and Dyes by Clay-Based Adsorbents: From Natural Clays to 1D and 2D Nano-Composites. *Chem. Eng. J.* **2021**, *420*, 127574. [CrossRef]
16. Marchesi, S.; Carniato, F.; Guidotti, M.; Botta, M.; Marchese, L.; Bisio, C. Synthetic Saponite Clays as Promising Solids for Lanthanide Ion Recovery. *New J. Chem.* **2020**, *44*, 10033–10041. [CrossRef]
17. Marchesi, S.; Nascimbene, S.; Guidotti, M.; Bisio, C.; Carniato, F. Application of NMR Relaxometry for Real-Time Monitoring of the Removal of Metal Ions from Water by Synthetic Clays. *Dalton Trans.* **2022**, *51*, 4502–4509. [CrossRef] [PubMed]
18. Novikau, R.; Lujaniene, G. Adsorption Behaviour of Pollutants: Heavy Metals, Radionuclides, Organic Pollutants, on Clays and Their Minerals (Raw, Modified and Treated): A Review. *J. Environ. Manag.* **2022**, *309*, 114685. [CrossRef]
19. Trujillano, R.; González, B.; Rives, V. Phase Change Materials (PCMs) Based in Paraffin/Synthetic Saponite Used as Heat Storage Composites. *Energies* **2021**, *14*, 7414. [CrossRef]
20. Costenaro, D.; Bisio, C.; Carniato, F.; Gatti, G.; Oswald, F.; Meyer, T.B.; Marchese, L. Size Effect of Synthetic Saponite-Clay in Quasi-Solid Electrolyte for Dye-Sensititized Solar Cells. *Sol. Energy Mater. Sol. Cells* **2013**, *117*, 9–14. [CrossRef]
21. Costenaro, D.; Gatti, G.; Carniato, F.; Paul, G.; Bisio, C.; Marchese, L. The Effect of Synthesis Gel Dilution on the Physico-Chemical Properties of Acid Saponite Clays. *Microporous Mesoporous Mater.* **2012**, *162*, 159–167. [CrossRef]
22. Vicente, I.; Salagre, P.; Cesteros, Y.; Medina, F.; Sueiras, J.E. Microwave-Assisted Synthesis of Saponite. *Appl. Clay Sci.* **2010**, *48*, 26–31. [CrossRef]
23. Zhang, D.; Zhou, C.-H.; Lin, C.-X.; Tong, D.-S.; Yu, W.-H. Synthesis of Clay Minerals. *Appl. Clay Sci.* **2010**, *50*, 1–11. [CrossRef]
24. Trujillano, R.; Rico, E.; Vicente, M.A.; Herrero, M.; Rives, V. Microwave Radiation and Mechanical Grinding as New Ways for Preparation of Saponite-like Materials. *Appl. Clay Sci.* **2010**, *48*, 32–38. [CrossRef]
25. Marchesi, S.; Guidotti, M.; Marchese, L.; Evangelisti, C.; Carniato, F.; Bisio, C. Bifunctional Europium(III) and Niobium(V)-Containing Saponite Clays for the Simultaneous Optical Detection and Catalytic Oxidative Abatement of Blister Chemical Warfare Agents. *Chem. A Eur. J.* **2021**, *27*, 4723–4730. [CrossRef]
26. Marchesi, S.; Bisio, C.; Carniato, F. Enhancement of the Luminescence Properties of Eu (III) Containing Paramagnetic Saponite Clays. *Appl. Sci.* **2021**, *11*, 8903. [CrossRef]
27. Marchesi, S.; Bisio, C.; Carniato, F. Novel Light-Emitting Clays with Structural Tb 3+ and Eu 3+ for Chromate Anion Detection. *RSC Adv.* **2020**, *10*, 29765–29771. [CrossRef]
28. Carniato, F.; Bisio, C.; Psaro, R.; Marchese, L.; Guidotti, M. Niobium(V) Saponite Clay for the Catalytic Oxidative Abatement of Chemical Warfare Agents. *Angew. Chem. Int. Ed.* **2014**, *53*, 10095–10098. [CrossRef]
29. Costenaro, D.; Bisio, C.; Carniato, F.; Safronyuk, S.L.; Kramar, T.V.; Taran, M.V.; Starodub, M.F.; Katsev, A.M.; Guidotti, M. Physico–Chemical Properties, Biological and Environmental Impact of Nb–Saponites Catalysts for the Oxidative Degradation of Chemical Warfare Agents. *ChemistrySelect* **2017**, *2*, 1812–1819. [CrossRef]

30. Marchesi, S.; Bisio, C.; Lalli, D.; Marchese, L.; Platas-Iglesias, C.; Carniato, F. Bifunctional Paramagnetic and Luminescent Clays Obtained by Incorporation of Gd3+ and Eu3+ Ions in the Saponite Framework. *Inorg. Chem.* **2021**, *60*, 10749–10756. [CrossRef]
31. Ostinelli, L.; Recchia, S.; Bisio, C.; Carniato, F.; Guidotti, M.; Marchese, L.; Psaro, R. Acid/Vanadium-Containing Saponite for the Conversion of Propene into Coke: Potential Flame-Retardant Filler for Nanocomposite Materials. *Chem. Asian J.* **2012**, *7*, 2394–2402. [CrossRef] [PubMed]
32. Carniato, F.; Bisio, C.; Gatti, G.; Roncoroni, S.; Recchia, S.; Marchese, L. On the Properties of a Novel V-Containing Saponite Catalyst for Propene Oxidative Dehydrogenation. *Catal. Lett.* **2009**, *131*, 42–48. [CrossRef]
33. Gil, A.; Santamaría, L.; Korili, S.A.; Vicente, M.A.; Barbosa, L.V.; de Souza, S.D.; Marçal, L.; de Faria, E.H.; Ciuffi, K.J. A Review of Organic-Inorganic Hybrid Clay Based Adsorbents for Contaminants Removal: Synthesis, Perspectives and Applications. *J. Environ. Chem. Eng.* **2021**, *9*, 105808. [CrossRef]
34. Liao, L.; Lv, G.; Cai, D.; Wu, L. The Sequential Intercalation of Three Types of Surfactants into Sodium Montmorillonite. *Appl. Clay Sci.* **2016**, *119*, 82–86. [CrossRef]
35. Bisio, C.; Carniato, F.; Paul, G.; Gatti, G.; Boccaleri, E.; Marchese, L. One-Pot Synthesis and Physicochemical Properties of an Organo-Modified Saponite Clay. *Langmuir* **2011**, *27*, 7250–7257. [CrossRef]
36. Lalli, D.; Marchesi, S.; Carniato, F.; Bisio, C.; Tei, L.; Marchese, L.; Botta, M. Combination of Solid-State NMR and 1H NMR Relaxometry for the Study of Intercalated Saponite Clays with the Macrocyclic Derivatives of Gd(III) and Y(III). *Dalton Trans.* **2020**, *49*, 6566–6571. [CrossRef]
37. Marchesi, S.; Carniato, F.; Bisio, C.; Tei, L.; Marchese, L.; Botta, M. Novel Paramagnetic Clays Obtained through Intercalation of Gd^{3+}-Complexes. *Dalton Trans.* **2018**, *47*, 7896–7904. [CrossRef]
38. Malheiro, R.; Casal, S.; Baptista, P.; Pereira, J.A. A Review of Bactrocera Oleae (Rossi) Impact in Olive Products: From the Tree to the Table. *Trends Food Sci. Technol.* **2015**, *44*, 226–242. [CrossRef]
39. Marchini, D.; Petacchi, R.; Marchi, S. Bactrocera Oleae Reproductive Biology: New Evidence on Wintering Wild Populations in Olive Groves of Tuscany (Italy). *Bull. Insectol.* **2017**, *70*, 121–128.
40. Malheiro, R.; Casal, S.; Cunha, S.C.; Baptista, P.; Pereira, J.A. Olive Volatiles from Portuguese Cultivars Cobrançosa, Madural and Verdeal Transmontana: Role in Oviposition Preference of Bactrocera Oleae (Rossi) (Diptera: Tephritidae). *PLoS ONE* **2015**, *10*, e0125070. [CrossRef]
41. Malheiro, R.; Ortiz, A.; Casal, S.; Baptista, P.; Pereira, J.A. Electrophysiological Response of Bactrocera Oleae (Rossi) (Diptera: Tephritidae) Adults to Olive Leaves Essential Oils from Different Cultivars and Olive Tree Volatiles. *Ind. Crops Prod.* **2015**, *77*, 81–88. [CrossRef]
42. Prieto, O.; Vicente, M.A.; Bañares-Muñoz, M.A. Study of the Porous Solids Obtained by Acid Treatment of a High Surface Area Saponite. *J. Porous Mater.* **1999**, *6*, 335–344. [CrossRef]
43. PubChem Hexanal. Available online: https://pubchem.ncbi.nlm.nih.gov/compound/6184 (accessed on 23 August 2022).
44. PubChem 2-Hexenal. Available online: https://pubchem.ncbi.nlm.nih.gov/compound/5281168 (accessed on 23 August 2022).
45. PubChem Heptanal. Available online: https://pubchem.ncbi.nlm.nih.gov/compound/8130 (accessed on 23 August 2022).
46. PubChem 2-Heptenal. Available online: https://pubchem.ncbi.nlm.nih.gov/compound/5283316 (accessed on 23 August 2022).
47. Smith, B.C. *Infrared Spectral Interpretation: A Systematic Approach*; CRC Press: Boca Raton, FL, USA, 1999; ISBN 978-0-8493-2463-5.
48. Osman, M.A.; Ernst, M.; Meier, B.H.; Suter, U.W. Structure and Molecular Dynamics of Alkane Monolayers Self-Assembled on Mica Platelets. *J. Phys. Chem. B* **2002**, *106*, 653–662. [CrossRef]
49. Takahashi, C.; Shirai, T.; Hayashi, Y.; Fuji, M. Study of Intercalation Compounds Using Ionic Liquids into Montmorillonite and Their Thermal Stability. *Solid State Ion.* **2013**, *241*, 53–61. [CrossRef]
50. Hlavatý, V.; Fajnor, V.Š. Thermal Stability of Clay/Organic Intercalation Complexes. *J. Therm. Anal. Calorim.* **2002**, *67*, 113–118. [CrossRef]
51. Paul, G.; Bisio, C.; Braschi, I.; Cossi, M.; Gatti, G.; Gianotti, E.; Marchese, L. Combined Solid-State NMR, FT-IR and Computational Studies on Layered and Porous Materials. *Chem. Soc. Rev.* **2018**, *47*, 5684–5739. [CrossRef]
52. Sacchetto, V.; Gatti, G.; Paul, G.; Braschi, I.; Berlier, G.; Cossi, M.; Marchese, L.; Bagatin, R.; Bisio, C. The Interactions of Methyl Tert-Butyl Ether on High Silica Zeolites: A Combined Experimental and Computational Study. *Phys. Chem. Chem. Phys.* **2013**, *15*, 13275–13287. [CrossRef]
53. Braschi, I.; Paul, G.; Gatti, G.; Cossi, M.; Marchese, L. Embedding Monomers and Dimers of Sulfonamide Antibiotics into High Silica Zeolite Y: An Experimental and Computational Study of the Tautomeric Forms Involved. *RSC Adv.* **2013**, *3*, 7427–7437. [CrossRef]
54. Ziyat, H.; Bennani, M.N.; Hajjaj, H.; Qabaqous, O.; Arhzaf, S.; Mekdad, S.; Allaoui, S. Adsorption of Thymol onto Natural Clays of Morocco: Kinetic and Isotherm Studies. *J. Chem.* **2020**, *2020*, 4926809. [CrossRef]
55. Nguemtchouin, M.G.M.; Ngassoum, M.B.; Chalier, P.; Kamga, R.; Ngamo, L.S.T.; Cretin, M. Ocimum Gratissimum Essential Oil and Modified Montmorillonite Clay, a Means of Controlling Insect Pests in Stored Products. *J. Stored Prod. Res.* **2013**, *52*, 57–62. [CrossRef]
56. Nguemtchouin, M.G.M.; Ngassoum, M.B.; Kamga, R.; Deabate, S.; Lagerge, S.; Gastaldi, E.; Chalier, P.; Cretin, M. Characterization of Inorganic and Organic Clay Modified Materials: An Approach for Adsorption of an Insecticidal Terpenic Compound. *Appl. Clay Sci.* **2015**, *104*, 110–118. [CrossRef]

57. Gueu, S.; Tia, V.E.; Bartier, D.; Barres, O.; Soro, F.D. Adsorption of Lippia Multiflora Essential Oil on Two Surfactant-Modified Clays: Qualitative Approach. *Clay Miner.* **2020**, *55*, 219–228. [CrossRef]
58. Giannakas, A.; Tsagkalias, I.; Achilias, D.S.; Ladavos, A. A Novel Method for the Preparation of Inorganic and Organo-Modified Montmorillonite Essential Oil Hybrids. *Appl. Clay Sci.* **2017**, *146*, 362–370. [CrossRef]
59. Giannakas, A.E.; Salmas, C.E.; Leontiou, A.; Moschovas, D.; Baikousi, M.; Kollia, E.; Tsigkou, V.; Karakassides, A.; Avgeropoulos, A.; Proestos, C. Performance of Thyme Oil@Na-Montmorillonite and Thyme Oil@Organo-Modified Montmorillonite Nanostructures on the Development of Melt-Extruded Poly-L-Lactic Acid Antioxidant Active Packaging Films. *Molecules* **2022**, *27*, 1231. [CrossRef]
60. Fernández, M.A.; Barberia Roque, L.; Gámez Espinosa, E.; Deyá, C.; Bellotti, N. Organo-Montmorillonite with Biogenic Compounds to Be Applied in Antifungal Coatings. *Appl. Clay Sci.* **2020**, *184*, 105369. [CrossRef]
61. Marçal, L.; de Faria, E.H.; Nassar, E.J.; Trujillano, R.; Martín, N.; Vicente, M.A.; Rives, V.; Gil, A.; Korili, S.A.; Ciuffi, K.J. Organically Modified Saponites: SAXS Study of Swelling and Application in Caffeine Removal. *ACS Appl. Mater. Interfaces* **2015**, *7*, 10853–10862. [CrossRef]
62. Hendry, P.; Ludi, A. Structure, Reactivity, Spectra, and Redox Properties of Cobalt(III) Hexaamines. In *Advances in Inorganic Chemistry*; Sykes, A.G., Ed.; Academic Press: Cambridge, MA, USA, 1990; Volume 35, pp. 117–198. [CrossRef]